

**Intrinsic magnetic properties in  $R(\text{Fe}_{1-x}\text{Co}_x)_{11}\text{TiZ}$  ( $R = \text{Y}$  and  $\text{Ce}$ ;  $Z = \text{H}$ ,  $\text{C}$ , and  $\text{N}$ )**Liqin Ke<sup>1,\*</sup> and Duane D. Johnson<sup>1,2</sup><sup>1</sup>Ames Laboratory, US Department of Energy, Ames, Iowa 50011, USA<sup>2</sup>Materials Science & Engineering, Iowa State University, Ames, Iowa 50011-2300, USA

(Received 7 May 2016; revised manuscript received 6 July 2016; published 19 July 2016)

To guide improved properties coincident with reduction of critical materials in permanent magnets, we investigate via density functional theory (DFT) the intrinsic magnetic properties of a promising system,  $R(\text{Fe}_{1-x}\text{Co}_x)_{11}\text{TiZ}$  with  $R = \text{Y}$ ,  $\text{Ce}$  and interstitial doping ( $Z = \text{H}$ ,  $\text{C}$ ,  $\text{N}$ ). The magnetization  $M$ , Curie temperature  $T_C$ , and magnetocrystalline anisotropy energy  $K$  calculated in local density approximation to DFT agree well with measurements. Site-resolved contributions to  $K$  reveal that all three Fe sublattices promote uniaxial anisotropy in  $\text{YFe}_{11}\text{Ti}$ , while competing anisotropy contributions exist in  $\text{YCo}_{11}\text{Ti}$ . As observed in experiments on  $R(\text{Fe}_{1-x}\text{Co}_x)_{11}\text{Ti}$ , we find a complex nonmonotonic dependence of  $K$  on Co content and show that anisotropy variations are a collective effect of MAE contributions from all sites and cannot be solely explained by preferential site occupancy. With interstitial doping, calculated  $T_C$  enhancements are in the sequence of  $\text{N} > \text{C} > \text{H}$ , with volume and chemical effects contributing to the enhancement. The uniaxial anisotropy of  $R(\text{Fe}_{1-x}\text{Co}_x)_{11}\text{TiZ}$  generally decreases with  $\text{C}$  and  $\text{N}$ ; although, for  $R = \text{Ce}$ ,  $\text{C}$  doping is found to greatly enhance it for a small range of  $0.7 < x < 0.9$ .

DOI: [10.1103/PhysRevB.94.024423](https://doi.org/10.1103/PhysRevB.94.024423)**I. INTRODUCTION**

The search for new permanent magnets without critical materials has generated great interest in the magnetism community [1,2]. Developing  $\text{CeFe}_{12}$ -based rare-earth ( $R$ )-transition-metal ( $TM$ ) intermetallics [3–7] is an important approach, considering the relative abundance of  $\text{Ce}$  among  $R$  elements and the large content of inexpensive  $\text{Fe}$ . To improve  $\text{CeFe}_{11}\text{Ti}$  as a permanent magnet, it is desired to modify the compound to achieve the best possible intrinsic magnetic properties, such as magnetization  $M$ , Curie temperature  $T_C$ , and magnetocrystalline anisotropy energy (MAE)  $K$ . Both substitutional doping with  $\text{Co}$  [8] and interstitial doping with small elements of  $\text{H}$ ,  $\text{C}$ , or  $\text{N}$  can strongly affect its magnetic properties. A theoretical understanding of intrinsic magnetic properties in this system and the effect of doping will help guide the experiments and help ascertain the best achievable permanent magnet properties.

Binary iron compounds of  $R\text{Fe}_{12}$  do not form for any  $R$  elements unless a small amount of stabilizer elements are added, such as  $T = \text{Ti}$ ,  $\text{Si}$ ,  $\text{V}$ ,  $\text{Cr}$ ,  $\text{Mo}$ , or  $\text{W}$  [9]. Such  $R\text{Fe}_{12-z}T_z$  compounds are generally regarded as ternaries rather than pseudobinaries because the third element,  $T$ , atoms often have a very strong site preference and exclusively sit at one of three nonequivalent  $\text{Fe}$  sites [10]. Magnetization often decreases quickly with the increase of  $T$  composition and a minimum amount of  $\text{Ti}$  ( $z = 0.7$ ) is needed to stabilize the structure, resulting in  $\text{Ti}$  compounds having better magnetic properties than others [11]. Prototype yttrium compounds are often studied to focus on the properties of the  $TM$  sublattices in the corresponding  $R\text{-}TM$  systems because yttrium can be regarded as a nonmagnetic, rare-earth element.

In comparison to other  $R\text{-Fe}$  systems [11,12], such as  $\text{Y}_2\text{Fe}_{17}$  and  $\text{Y}_2\text{Fe}_{14}\text{B}$ ,  $\text{Fe}$  sublattices in 1-12 compounds have relative low magnetization due to a more compact

structure, but at low temperatures a very high uniaxial MAE, e.g.,  $K = 2 \text{ MJm}^{-3}$  in  $\text{YFe}_{11}\text{Ti}$  [8,13]. Curie temperatures are relatively low;  $M$  and  $K$  quickly decrease with increasing temperature [14–16].  $\text{CeFe}_{11}\text{Ti}$  has  $T_C \approx 485 \text{ K}$ , and a low-temperature magnetization within a range of  $17.4\text{--}20.2 \mu_B/\text{f.u.}$ , while  $\text{YFe}_{11}\text{Ti}$  has a slightly larger  $M$  and  $T_C$ . At room temperature,  $\text{CeFe}_{11}\text{Ti}$  has a larger  $K$  ( $1.3 \text{ MJm}^{-3}$ ) than  $\text{YFe}_{11}\text{Ti}$  ( $0.89 \text{ MJm}^{-3}$ ). This may indicate that the  $\text{Ce}$  sublattice has a positive contribution to the uniaxial anisotropy [15].

The substitutional doping with  $\text{Co}$  is a common approach to improve  $T_C$  in  $R\text{-Fe}$  compounds [8]. Pure phase  $R(\text{Fe}_{1-x}\text{Co}_x)_{11}\text{Ti}$  exists over the whole composition range for both  $R = \text{Y}$  and  $\text{Ce}$  [17]. The largest magnetization in  $\text{Y}(\text{Fe}_{1-x}\text{Co}_x)_{11}\text{Ti}$  occurs at  $\text{YFe}_8\text{Co}_3\text{Ti}$  while the  $T_C$  increases continuously with  $\text{Co}$  composition until it reaches the maximum in  $\text{YCo}_{11}\text{Ti}$  [18,19]. For  $\text{Ce}$  compounds, the maximum  $T_C$  is obtained in  $\text{CeFe}_2\text{Co}_9\text{Ti}$  [17]. The dependence of MAE on the  $\text{Co}$  composition in  $R(\text{Fe}_{1-x}\text{Co}_x)_{11}\text{Ti}$  is more intriguing and not understood. Although early experiments [8,14] suggested that  $\text{YCo}_{11}\text{Ti}$  has a planar anisotropy, later experiments agreed that  $\text{YCo}_{11}\text{Ti}$  has uniaxial anisotropy [17–23] but with a magnitude smaller than those of  $\text{YFe}_{11}\text{Ti}$ . For the intermediate  $\text{Co}$  composition, anisotropy changes from uniaxial to planar and then back to uniaxial with the increase of  $\text{Co}$  composition in both  $\text{Y}(\text{Fe}_{1-x}\text{Co}_x)_{11}\text{Ti}$  and  $\text{Ce}(\text{Fe}_{1-x}\text{Co}_x)_{11}\text{Ti}$  [17–23].

The interstitial doping with  $\text{H}$  [15],  $\text{N}$  [5,24,25], and  $\text{C}$  [26–28] can increase  $M$  and  $T_C$  and provide control of the magnitude and sign of the MAE constants in  $R\text{Fe}_{11}\text{Ti}$ . Hydrogenation simultaneously increases all three intrinsic magnetic properties in  $\text{YFe}_{11}\text{Ti}$ , and enhancements are  $\Delta M = 1 \mu_B/\text{f.u.}$  at  $4.2 \text{ K}$ ,  $\Delta T_C = 60 \text{ K}$  [16,29], and  $\Delta K = 6.5\%$  [16], respectively. Insertion of larger  $\text{C}$  and  $\text{N}$  atoms has a much stronger effect on the enhancements of  $M$  and  $T_C$  [27,30]. Unfortunately, it is achieved at the expense of uniaxial anisotropy. In comparison with  $\text{YFe}_{11}\text{Ti}$ , enhancements of  $\Delta M = 2.6 \mu_B/\text{f.u.}$  and  $\Delta T_C = 154 \text{ K}$  were observed in  $\text{YFe}_{11}\text{TiC}_{0.9}$ , and  $\Delta M = 2.7 \mu_B/\text{f.u.}$  and  $\Delta T_C = 218 \text{ K}$  in  $\text{YFe}_{11}\text{TiN}_{0.8}$ . The MAE decreases

\*liqinke@ameslab.gov

by  $\Delta K = 0.6 \sim 0.7 \text{ MJm}^{-3}$  in both compounds. Doping influences the MAE contributions from both  $TM$  sublattice and rare-earth atoms. It had been argued that the proximity of doping atoms to the rare-earth atoms in  $R\text{TiFe}_{11}\text{N}_x$  may lead to drastic changes in the rare-earth sublattice anisotropy [25], and N doping often has an opposite effect on MAE as H doping [30]. For Ce compounds, a similar amount of  $T_C$  enhancement was obtained upon nitriding [5], and the effect of H doping is much smaller. Isnard *et al.* [15] found that not much change is observed upon H insertion either in the room temperature anisotropy or in saturation magnetization.

Other possible interstitial doping elements such as B, Si, or P atoms are much less favored to occupy the interstitial sites due to chemical or structural reasons [26]. In fact, interestingly, it has been found that the B atoms prefer to substitute for some of the Ti atoms and drive the Ti into the interstitial [31].

The nature of the Ce  $4f$  state different Ce- $TM$  compounds is often a controversial subject [32]. The anomalies in the lattice constants as well as the magnetic moment and Curie temperature have been interpreted as evidence of the mixed-valence (between  $\text{Ce}^{3+}$  and  $\text{Ce}^{4+}$ ) behavior of the cerium ion. It is further complicated by the doping. Controversy remains on how Ce valence states are affected upon hydrogenation [15,33]. It also has been shown that Ce  $4f$  states are itinerant and, as such, the standard localized  $4f$  picture is not appropriate for systems such as  $\text{CeCo}_5$  [34,35]. Moreover, in the  $(\text{Nd-Ce})_2\text{Fe}_{14}\text{B}$  system, the mixed valency of Ce has been shown to be due to local site volume and site chemistry effects [36]. In this paper the  $4f$  states in Ce are treated as itinerant and included as valence states, and we found that magnetic properties calculated are in good agreement with experiments.

## II. CALCULATION DETAILS

### A. Crystal structure

$R\text{Fe}_{11}\text{Ti}$  has a body-center-tetragonal  $\text{ThMn}_{12}$ -type ( $I4/mmm$  space group, no. 139) structure, which is closely related to the 1-5 and 2-17  $R$ - $TM$  structures [11]. The primitive unit cell contains one formula unit (f.u.). As shown in Fig. 1,  $R$  atoms occupy the  $2a(4/mmm)$  site, while transition metal atoms are divided into three sublattices,  $8i(m2m)$ ,  $8j(m2m)$ , and  $8f(2/m)$ , each of which has fourfold multiplicities. The  $8j$  and  $8f$  sites bear a great similarity in their local environments with respect to the distribution of coordinated atoms [37], whereas the  $8i$  sites, often referred to as dumbbell sites, form -Fe-Fe- $R$ - chains with  $R$  atoms along the basal axes, instead of the  $c$  axis, as in the 2-17 structure [38]. Ti atoms occupy nearly exclusively on the  $8i$  sites, however, the distribution of Fe and Ti atoms within the  $8i$  sites is disordered.

To calculate  $R\text{Fe}_{11}\text{Ti}$ , we replace one of four Fe( $8i$ ) atoms with Ti in the primitive cell of  $R\text{Fe}_{12}$  and neglect the effect of the artificial Ti ordering introduced by using this unit cell. Although the  $I4/mmm$  symmetry is lowered by Ti substitution or the spin-orbit coupling (SOC) in the anisotropy calculation, we still use the notations of  $8j$ ,  $8i$ , and  $8f$  sites for simplicity.

For Co doping, Mössbauer spectroscopy found that Co atoms preferentially occupy the  $8f$  sites in  $\text{Y}(\text{Fe}_{1-x}\text{Co}_x)_{11}\text{Ti}$  [39], while the high-resolution neutron

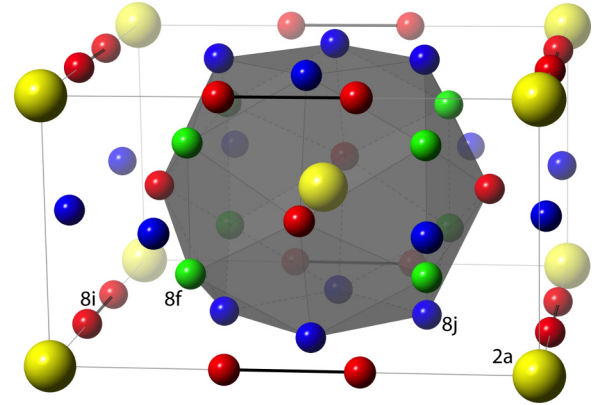


FIG. 1. Schematic representation of the crystal structures of  $R\text{Fe}_{11}\text{Ti}$ .  $R(2a)$  atoms are indicated with larger spheres in yellow color. Three transition metal sublattices  $8i$ ,  $8j$ , and  $8f$  are in red, blue, and green, respectively. Each  $R$  atom has four nearest  $8i$ , eight nearest  $8j$ , and  $8f$  neighbor atoms. Among three  $TM$  sites, the  $8i$  site has the shortest distance from the  $R$  atom. Interstitial sites  $2b$  (not shown) are halfway between two  $R$  atoms along the  $c$  axis and coordinated by an octahedron of two  $R$  and four Fe( $8j$ ) sites.

powder diffraction experiments concluded that Co atoms preferentially occupy sites in the sequence of  $8j > 8f > 8i$  [40]. For interstitial H, C, and N doping, neutron scattering has shown that dopants prefer to occupy the larger octahedral  $2b$  interstitial sites [15,25], which have the shortest distance from the rare-earth sites among all empty interstitial sites. In all our calculations, we also assume that H, C, or N atom occupies the  $2b$  sites.

### B. Computational methods

Most magnetic properties were calculated using a standard linear muffin-tin orbital (LMTO) basis set [41] generalized to full potentials [42]. This scheme employs generalized Hankel functions as the envelope functions. For MAE calculation, the SOC was included through the force theorem [43]. The MAE is defined below as  $K = E_{110} - E_{001}$ , where  $E_{001}$  and  $E_{110}$  are the summation of band energies for the magnetization being oriented along the  $[001]$  and  $[110]$  directions, respectively. Positive (negative)  $K$  corresponds to uniaxial (planar) anisotropy. It should be noted that, due to the presence of Ti in the primitive cell, the two basal axes become inequivalent, with -Ti-Fe- $R$ - chains along the  $[100]$  direction and -Fe-Fe- $R$ - chains along the  $[010]$  direction.  $E_{100}$  and  $E_{010}$  become different, which is an artifact introduced by using the small primitive cell and artificial ordering of Ti within the  $8i$  sublattice.

We found that the  $[100]$  direction is harder than the  $[010]$  in  $\text{YFe}_{11}\text{Ti}$ , and vice versa in  $\text{YCo}_{11}\text{Ti}$ .  $E_{110}$  is usually about the average of  $E_{100}$  and  $E_{010}$ . Thus, we use  $[110]$  as the reference direction for the basal plane. A  $16 \times 16 \times 16$   $k$ -point mesh is used for MAE calculations to ensure sufficient convergence; MAE in  $\text{YFe}_{11}\text{Ti}$  changed by less than 3% when a denser  $32 \times 32 \times 32$  mesh was employed. To decompose the MAE, we evaluate the on-site SOC matrix element  $\langle V_{\text{so}} \rangle$  and the corresponding anisotropy  $K_{\text{so}} = \frac{1}{2} \langle V_{\text{so}} \rangle_{110} - \frac{1}{2} \langle V_{\text{so}} \rangle_{001}$ . Unlike MAE,  $K_{\text{so}}$  can be easily decomposed into sites, spins, and orbital pairs. According to second-order perturbation

theory [44,45],

$$K \approx \sum_i K_{\text{so}}(i), \quad (1)$$

where  $i$  indicates atomic sites. Equation (1) holds true for all compounds that we investigated in this paper. Hence, we use  $K_{\text{so}}(i)$  to represent the site-resolved MAE. For simplicity, we write it as  $K(i)$ .

Exchange coupling parameters  $J_{ij}$  are calculated using a static linear-response approach implemented in a Green's function (GF) LMTO method, simplified using the atomic sphere approximation (ASA) to the potential and density [46,47]. The scalar-relativistic Hamiltonian was used so SOC is not included, although it is a small perturbation on  $J_{ij}$ 's. In the basis set,  $s, p, d, f$  orbitals are included for Ce, Y, Fe, and Co atoms, and  $s, p$  orbitals are included for H, C, and N atoms. Exchange parameters  $J_{ij}(\mathbf{q})$  are calculated using a  $16^3$   $k$ -point mesh, and  $J_{ij}(\mathbf{R})$  can be obtained by a subsequent Fourier transforming.  $T_C$  is estimated in the mean-field approximation (MFA) or random-phase approximation (RPA). See Ref. [46] for details of the methods to calculate  $T_C$ .

For all magnetic property calculations, the effective one-electron potential was obtained within the local density approximation (LDA) to DFT using the parametrization of von Barth and Hedin [48]. However, with the functional of Perdew, Becke, and Ernzerhof (PBE) being better at structural relaxation for most of the solids containing  $3d$  elements [49], we use it to fully relax the lattice constants and internal atomic positions in a fast plane-wave method, as implemented within the Vienna *ab initio* simulation package (VASP) [50,51]. The nuclei and core electrons were described by the projector augmented wave (PAW) potential [52] and the wave functions of valence electrons were expanded in a plane-wave basis set with a cutoff energy of up to 520 eV. All relaxed structures are then verified in FP-LMTO before the magnetic property calculations are performed.

### III. RESULTS AND DISCUSSION

#### A. Structure

Lattice constants and volumes are listed in Table I; the calculated lattice constants are in good agreement with experiments. The strong Ti site preference on the  $8i$  site [3,15,54] had been interpreted in terms of atomic volume, coordination number, and enthalpy. It had been argued that enthalpy associated with  $R$  and Ti, V, or Mo atoms are positive and  $8i$  sites have the smallest contact area with  $R$  atoms. To identify quantitatively the site-preference effect, we calculated the total energy of  $\text{CeFe}_{11}\text{Ti}$  with one Ti atom occupying at the  $8i$ ,  $8j$ , or  $8f$  sites, respectively, in the 13-atom primitive cell. The lowest-energy structure is the one with Ti atoms on the  $8i$  site. Energies are higher by 42 meV/atom and 60 meV/atom with Ti atom being on the  $8j$  and  $8f$  sites, respectively. Hence, Ti atom should have a strong preference to occupy the  $8i$  sites, as observed in the experiments.

In comparison to the hypothetical 1-12 compounds, the replacement of Fe or Co atoms with Ti increases volume by 1% or 2%, respectively. Experimentally, H doping slightly increases the volume by 1% in  $\text{YFe}_{11}\text{TiH}$ , which is not observed in our calculation. The calculated volume of

TABLE I. Calculated and measured (Expt.) values for the lattice parameters and volume are listed for various compounds.

Compounds	$a^a$ (Å)	$c$ (Å)	$V$ (Å <sup>3</sup> )	$\Delta V/V$	Ref.
$\text{YFe}_{11}\text{Ti}$ (Expt.)	8.480	4.771	343.08		[53]
$\text{YFe}_{11}\text{Ti}$	8.472	4.720	338.78	0	
$\text{YFe}_{12}$	8.447	4.695	334.94	-1.1	
$\text{YFe}_{11}\text{TiH}$	8.457	4.732	338.43	-0.10	
$\text{YFe}_{11}\text{TiC}$	8.517	4.834	350.67	3.51	
$\text{YFe}_{11}\text{TiN}$	8.563	4.791	351.31	3.70	
$\text{YCo}_{11}\text{Ti}$ (Expt.)	8.367	4.712	329.87		[54]
$\text{YCo}_{11}\text{Ti}$	8.328	4.673	324.08	0	
$\text{YCo}_{12}$	8.268	4.655	318.21	-1.81	
$\text{YCo}_{11}\text{TiH}$	8.343	4.688	326.30	0.68	
$\text{YCo}_{11}\text{TiC}$	8.396	4.767	336.08	3.70	
$\text{YCo}_{11}\text{TiN}$	8.436	4.716	335.59	3.55	
$\text{CeFe}_{11}\text{Ti}$ (Expt.)	8.539	4.780	348.53		[15]
$\text{CeFe}_{11}\text{Ti}$	8.524	4.670	339.35	0	
$\text{CeFe}_{12}$	8.504	4.648	336.12	-0.95	
$\text{CeFe}_{11}\text{TiH}$	8.498	4.738	342.13	0.82	
$\text{CeFe}_{11}\text{TiC}$	8.501	4.891	353.45	4.16	
$\text{CeFe}_{11}\text{TiN}$	8.570	4.809	353.17	4.07	
$\text{CeCo}_{11}\text{Ti}$ (Expt.)	8.380	4.724	331.74		[17]
$\text{CeCo}_{11}\text{Ti}$	8.360	4.657	325.46	0	
$\text{CeCo}_{12}$	8.291	4.648	319.51	-1.82	
$\text{CeCo}_{11}\text{TiH}$	8.359	4.694	327.94	0.76	
$\text{CeCo}_{11}\text{TiC}$	8.383	4.811	338.07	3.87	
$\text{CeCo}_{11}\text{TiN}$	8.442	4.735	337.44	3.68	

<sup>a</sup>Except for the hypothetical 1-12 compounds, Ti substitution in the 13-atom cell breaks the symmetry of  $\text{CeFe}_{12}$ , and lattice parameters  $a$  and  $b$  become nonequivalent. The listed calculated  $a$  is an average of  $a$  and  $b$  of the unit cell used in the calculation.

$\text{CeFe}_{11}\text{TiH}$  is 0.82% larger than  $\text{CeFe}_{11}\text{Ti}$ . Calculations show that carbonizing and nitriding have a larger effect on volume expansion than hydrogenation and volume expansion is larger in Ce compounds than in Y compounds, both of which agree with experiments.

The total density of states of  $\text{YFe}_{11}\text{Ti}$  and  $\text{YFe}_{11}\text{TiN}$  compares reasonably well with previously reported LMTO-ASA calculations [6]. Figure 2 shows the scalar-relativistic partial density of states (PDOS) projected on individual elements in  $\text{YFe}_{11}\text{Ti}$ ,  $\text{YFe}_{11}\text{TiH}$ ,  $\text{YFe}_{11}\text{TiC}$ , and  $\text{YFe}_{11}\text{TiN}$ . The Fe PDOS are averaged over 11 Fe atoms. The interstitial doping elements on  $2b$  sites hybridizes with neighboring  $R$  and  $\text{Fe}(8j)$  atoms. H- $s$  states hybridize with neighboring Y and  $\text{Fe}(8j)$  atoms at around -7 eV below the Fermi level in  $\text{YFe}_{11}\text{TiH}$ . The C- $p$  and N- $p$  states have larger energy dispersion in  $\text{YFe}_{11}\text{TiC}$  and  $\text{YFe}_{11}\text{TiN}$ , respectively. The Fe states hybridized with interstitial elements, as shown in Fig. 2, are mostly from four ( $8j$ ) out of 11 Fe sites.  $\text{Fe}(8f)$  sites are the furthest away from the interstitial  $2b$  sites and their hybridization with doping elements are negligible. The Ce compounds have large  $f$  states above the Fermi level and share lots of similar PDOS features with the corresponding Y compounds below the Fermi level.

#### B. Magnetization, exchange couplings, and $T_C$

Intrinsic magnetic properties of each compound are listed in Table II. Experimental magnetization and anisotropy values



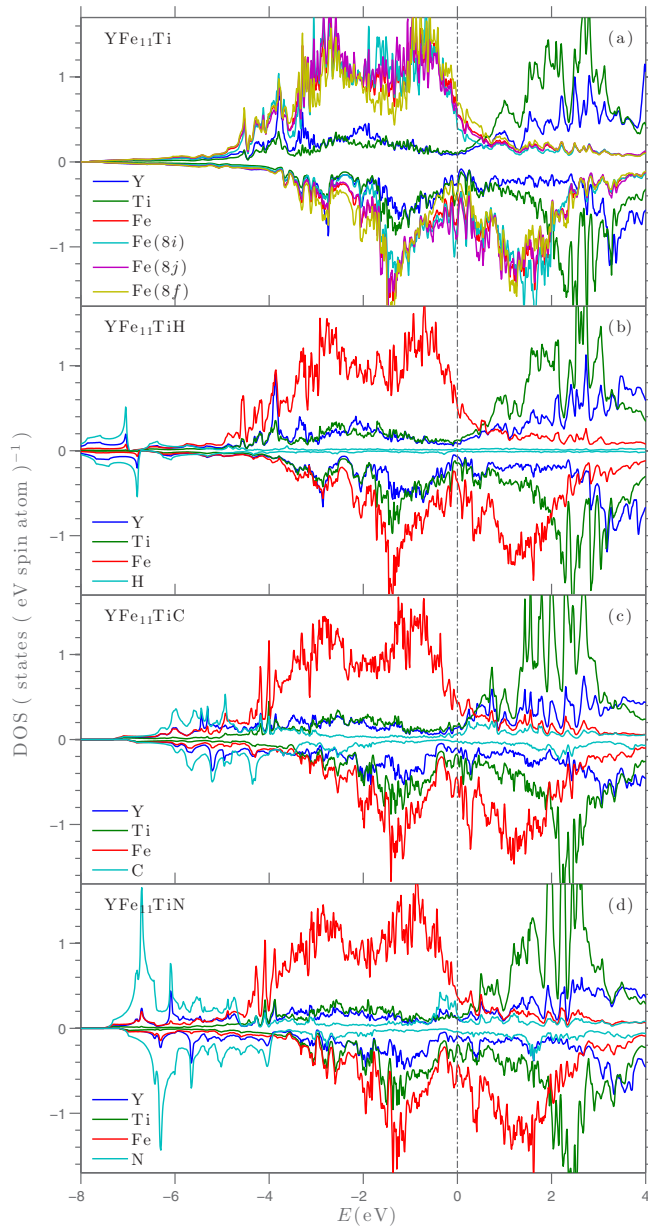


FIG. 2. Atom- and spin-projected partial densities of states (DOS) in (a)  $\text{YFe}_{11}\text{Ti}$ , (b)  $\text{YFe}_{11}\text{TiH}$ , (c)  $\text{YFe}_{11}\text{TiC}$ , and (d)  $\text{YFe}_{11}\text{TiN}$  within the LDA and no SOC. For  $\text{YFe}_{11}\text{Ti}$ , the Fe DOS are further resolved by averaging states projected on  $8i$ ,  $8j$ , and  $8f$  sites. Majority spin (positive values) and minority spin (negative values) DOS are shown separately. Fermi energy  $E_F$  is at 0 eV.

vary. The calculated magnetizations in  $\text{YFe}_{11}\text{Ti}$ ,  $\text{YCo}_{11}\text{Ti}$ , and  $\text{CeFe}_{11}\text{Ti}$  compare well with experiments. For  $\text{CeCo}_{11}\text{Ti}$ , only a limited number of studies had been reported, and the calculated magnetization is larger than experimental ones. Ti spin moments couple antiparallel to those of Fe and Co sublattices, which is typical for the light  $3d$  and  $4d$  elements [56]. In  $\text{CeFe}_{11}\text{Ti}$ , the Ce spin moments antiferromagnetically couple with the  $TM$  sublattice as expected [57]. Ce has a spin moment  $m_s \approx -0.7 \mu_B$  and an orbital moment  $m_l \approx 0.3 \mu_B$  with the opposite sign, which reflects Hund's third rule. The calculated Fe spin moments on the individual sublattice have

the magnitude in the sequence of  $m_s(8i) > m_s(8j) > m_s(8f)$ , which agrees with previous experiments and calculations [58]. The dumbbell  $8i$  sites have larger spin magnetic moments because of the relative larger surrounding empty volume and smaller atomic coordination number. The orbital magnetic moments calculated are larger in the Co-rich compounds than the Fe-rich compounds. MFA overestimated  $T_C$  by about 200 K in Fe compounds and about 50–100 K in Co compounds, respectively. RPA gives lower  $T_C$  values, e.g., 489 K in  $\text{YFe}_{11}\text{Ti}$ , and 461 K in  $\text{CeFe}_{11}\text{Ti}$ , respectively. The experimental  $T_C$  falls between the MFA and RPA values, and is much closer to the latter.

Ti additions decrease the magnetization by 20% in  $R\text{Fe}_{11}\text{Ti}$  and  $R\text{Co}_{11}\text{Ti}$  relative to their 1-12 hypothetical counterparts. The magnetization reduction is not only due to the replacement of ferromagnetic Fe by antiferromagnetic Ti atoms (spin moment  $-0.54 \mu_B$ ) but also the suppression of the ferromagnetism on the neighboring Fe sublattices. This is a common effect of doping early  $3d$  or  $4d$  elements on the Fe or Co sublattice [56]. On the other hand, the addition of the Ti atom barely affects the Ce moment. Interestingly, although magnetization decreased by 20% upon the Ti addition, the calculated  $T_C$  is even slightly higher in  $\text{YFe}_{11}\text{Ti}$  than in  $\text{YFe}_{12}$ . This is somewhat reflected in the experiments, in which no obvious  $T_C$  dependence on Ti composition was observed in  $\text{YFe}_{11-z}\text{Ti}_z$  over the homogeneous 1-12 phase composition range,  $0.7 \leq z \leq 1.25$  [11].

To understand this phenomenon, we investigated the effective exchange coupling parameters  $J_0(i) = \sum_j J_{ij}$  and compare  $J_0$  values in  $\text{YFe}_{12}$  and  $\text{YFe}_{11}\text{Ti}$ . With Ti replacing one Fe atom,  $J_0$  values increase for all sites except the pair of Ti-Fe dumbbell sites. The overall  $J_0$  and the mean-field  $T_C$  increase. The site-resolved effective exchange parameters  $J_0(i)$  for various compounds are listed in Table II.

Figure 3 shows the magnetization as a function of the Co composition in  $\text{YFe}_{11}\text{Ti}$ , with similar behavior to the Slater-Pauling curve. The maximum magnetization occurs at  $x = 0.2$ , while in experiments it is at  $x = 0.3$  [19]. Similarly, for  $\text{Ce}(\text{Fe}_{1-x}\text{Co}_x)_{11}\text{Ti}$ , the experimental maximum magnetization occurs at  $x = 0.1-0.15$  [55]. As shown in Table II, the  $R\text{Co}_{11}\text{Ti}$  compounds have much larger  $T_C$  than the corresponding  $R\text{Fe}_{11}\text{Ti}$  compounds, which agrees with experiments [17].

All interstitial doping increases  $M$  and  $T_C$  in  $\text{YFe}_{11}\text{Ti}$  and  $\text{CeFe}_{11}\text{Ti}$ , and nitriding has the strongest effect. With H, C, and N doping, the calculated Curie temperature in  $\text{YFe}_{11}\text{Ti}$  increases by 51, 157, and 211 K, respectively, which is consistent with experiments.  $J_0$  values on all three  $TM$  sublattices increase with interstitial doping. Although DFT underestimates the volume expansion with H doping, the calculated  $\Delta T_C$  is only slightly smaller than the experimental value. The calculated  $\Delta T_C$  is larger with N doping than C doping, while their calculated volume expansions are similar. This indicates that both volume and chemical effects are important for the  $T_C$  enhancement. To estimate qualitatively the relative magnitudes of the two effects, we calculate the  $T_C$  of several hypothetical compounds related to  $\text{YFe}_{11}\text{TiN}$  by removing the N atom in the unit cell or replacing it with H or C atoms, respectively. The calculated  $\Delta T_C$  of those structures relative to  $\text{YFe}_{11}\text{Ti}$  are 53, 80, and 169 K, respectively. Obviously, both volume and chemical effects contribute to

TABLE II. Calculated spin  $M_s$ , orbital  $M_l$ , and total  $M_t$  magnetization, exchanges  $J_0$ , Curie temperature  $T_C$  estimated in the mean-field approximation, and magnetocrystalline anisotropy  $K$  in various compounds. Unless specified, experimental magnetization and anisotropy  $K$  values from previous studies were measured or evaluated for low temperature ( $<5$  K).

Compound	$M_s$	$M_l$	$M_t$	$J_0$ (meV)					$T_C$	$\Delta T_C$	$K$		Ref.
				$8i$ (Ti)	$8i$	$8j$	$8f$	Y			K	( $\frac{\text{meV}}{\text{f.u.}}$ )	
YFe <sub>12</sub>	24.20	0.61	24.81		7.57	4.91	5.10	1.34	689	-38	1.40	1.34	
YFe <sub>11</sub> Ti (Expt.)			19–20.6						524–538			2.0	[8,11,16,19,27]
YFe <sub>11</sub> Ti	19.75	0.60	20.35	5.29	7.17	6.70	6.61	1.43	727	0	1.93	1.83	
YFe <sub>11</sub> TiH	19.92	0.54	20.46	4.99	7.63	7.46	7.57	1.40	778	51	2.07	1.96	
YFe <sub>11</sub> TiC	20.64	0.55	21.19	5.51	8.58	8.83	8.66	1.67	884	157	0.95	0.87	
YFe <sub>11</sub> TiN	22.11	0.57	22.68	5.44	9.36	8.91	9.29	1.30	938	211	1.80	1.65	
YCo <sub>11</sub> Ti (Expt.)			14.2–15.7						1020–1050			0.75 <sup>a</sup>	[18,19]
YCo <sub>11</sub> Ti	14.42	0.82	15.24	3.93	10.50	10.13	11.13	1.45	1091	364	0.94	0.93	
YCo <sub>12</sub>	18.42	0.90	19.32		12.52	13.12	13.84	1.66	1374	647	0.48	0.48	
CeFe <sub>12</sub>	24.02	0.78	24.80		8.69	7.33	6.12	1.75	806	131	1.77	1.69	
CeFe <sub>11</sub> Ti (Expt.)			17.4–20.2						482–487			1.3 <sup>a</sup> –2.0 <sup>a</sup>	[5,15,17,18,55]
CeFe <sub>11</sub> Ti	19.19	0.72	19.91	4.69	6.26	7.04	5.95	2.16	675	0	2.09	1.98	
CeFe <sub>11</sub> TiH	20.24	0.77	21.01	4.67	6.87	7.42	7.04	2.30	736	61	2.03	1.90	
CeFe <sub>11</sub> TiC	19.84	0.73	20.57	5.45	9.86	8.62	8.62	3.44	908	233	1.09	0.99	
CeFe <sub>11</sub> TiN	21.48	0.67	22.15	5.51	9.09	8.53	8.99	1.09	905	230	1.78	1.62	
CeCo <sub>11</sub> Ti (Expt.)			10.9–12.53 <sup>a</sup>						920–937			Axial	[17,18]
CeCo <sub>11</sub> Ti	13.77	1.32	15.09	4.07	10.40	9.38	10.94	3.76	1044	369	1.29	1.23	
CeCo <sub>12</sub>	17.35	1.36	18.71		12.03	12.29	12.97	3.80	1286	611	1.24	1.24	

<sup>a</sup>Measured at room temperature.

the  $T_C$  enhancement, and the chemical effects of interstitial elements are in the sequence of  $N > C > H$ .

### C. MAE in $R(\text{Fe}_{1-x}\text{Co}_x)_{11}\text{Ti}$

As listed in Table II, both YFe<sub>11</sub>Ti and YCo<sub>11</sub>Ti have uniaxial anisotropy. Calculated MAE in YFe<sub>11</sub>Ti is in good agreement with the experimental value. CeFe<sub>11</sub>Ti has a slightly larger MAE than YFe<sub>11</sub>Ti as found in experiments [15,32]. The PBE functional (not shown) gives a smaller MAE than LDA in YFe<sub>11</sub>Ti and CeFe<sub>11</sub>Ti.

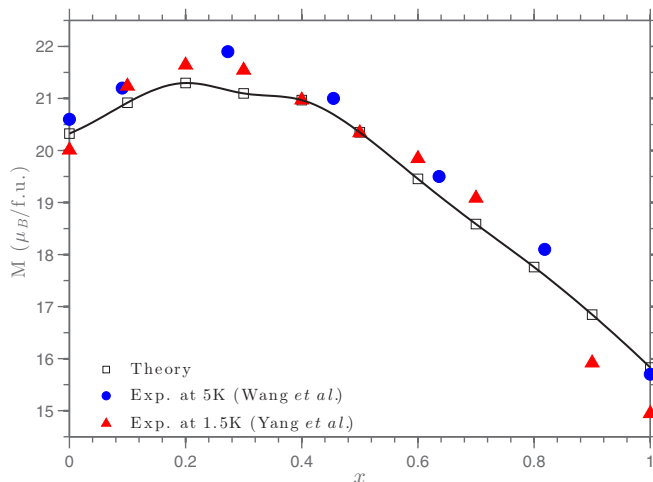


FIG. 3. Comparison of measured and calculated (squares)  $M$  versus Co content in  $\text{Y}(\text{Fe}_{1-x}\text{Co}_x)_{11}\text{Ti}$ . Experimental data are from Wang *et al.* [19] at 5 K (circles) and Yang *et al.* [8] at 1.5 K (triangles).

The Fe sublattice anisotropy may have a strong dependence on the composition of stabilizer atoms [14]. To understand how Ti affects the magnetic anisotropy and the origin of the nonmonotonic dependence of MAE on Co composition, we resolved MAE into sites by evaluating the matrix element of the on-site SOC energy [44,45]. For intermediate Co composition, we investigate the MAE in YFe<sub>7</sub>Co<sub>4</sub>Ti and YFe<sub>3</sub>Co<sub>8</sub>Ti. We calculated the formation energy relative to YFe<sub>11</sub>Ti and YCo<sub>11</sub>Ti and found that YFe<sub>7</sub>Co<sub>4</sub>Ti has a formation energy  $E_{\text{fmm}} = -34$  meV/atom with four Co atoms on the  $8j$  sites and  $E_{\text{fmm}} = -28$  meV/atom with four Co atoms on the  $8f$  sites. Both values are lower than  $E_{\text{fmm}} = -10$  meV/atom, the formation energy of YFe<sub>8</sub>Co<sub>3</sub>Ti with all three Co atoms being on the  $8i$  sites. Hence, the site preference of Co atoms is  $8j > 8f > 8i$ , which agrees with the neutron scattering experiments [40]. For YFe<sub>3</sub>Co<sub>8</sub>Ti, we occupy another four Co atoms on the  $8f$  sites and the corresponding formation energy is  $-31$  meV/atom.

Figure 4 shows the total MAE values and their sublattice-resolved components, in YFe<sub>12</sub>, YFe<sub>7</sub>Co<sub>4</sub>Ti, YFe<sub>3</sub>Co<sub>8</sub>Ti, and YCo<sub>11</sub>Ti. Obviously, Eq. (1) is well satisfied in all compounds and  $K_{\text{so}}$  presents well the site-resolved MAE. The Y sublattice has a negligible contribution to anisotropy, as expected for a weakly magnetic atom, because the spin-parallel components of MAE contribution cancel out the spin-flip ones [45]. Sublattice-resolved MAE contributions in YFe<sub>12</sub> shows  $K(8j) > K(8i) > 0 > K(8f)$ , which agrees with the previous estimation in sign but differs in the order [11]. Considering Fe( $8i$ ) sites have positive contributions to the uniaxial anisotropy in YFe<sub>12</sub>, one may expect that replacing Fe atoms by the Ti atoms on the  $8i$  site would decrease MAE. Interestingly, we found that YFe<sub>11</sub>Ti has even larger uniaxial anisotropy than YFe<sub>12</sub>. Anisotropies of all three sublattices

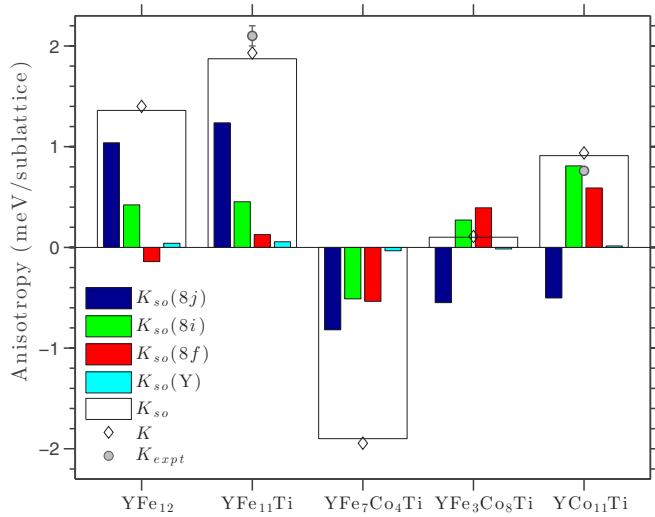


FIG. 4. Total and sublattice-resolved  $K_{so}$  in  $YFe_{11}Ti$ ,  $YFe_7Co_4Ti$ ,  $YFe_3Co_8Ti$ , and  $YCo_{11}Ti$ . Calculated  $K$  and measured  $K_{expt}$  values are also compared. Experimental values were from Refs. [29] and [18], measured at 4.2 K for  $YFe_{11}Ti$  and 293 K for  $YCo_{11}Ti$ , respectively. In calculations, we assume that all four Co occupy the  $8j$  sites in  $YFe_7Co_4Ti$  while all eight Co occupy the  $8j$  and  $8f$  sites in  $YFe_3Co_8Ti$ .

become more uniaxial and  $K(8j) > K(8i) > K(8f) > 0$  in  $YFe_{11}Ti$ , which indicates that the introduction of Ti atoms modifies the electronic structure of neighboring sites and enhances their contribution to uniaxial anisotropy. Similarly, other compounds, such as  $YCo_{11}Ti$ ,  $CeFe_{11}Ti$ , and  $CeCo_{11}Ti$ , are also found to have MAE values larger than or similar to their corresponding hypothetical 1-12 counterparts.

The dependence of MAE on the Co composition is nonmonotonic and also found in other  $R-TM$  systems [59]. As shown in Fig. 4, the calculated MAE reproduce the trend observed in experiment. For intermediate Co compositions,  $YFe_7Co_4Ti$  compound has planar anisotropy while  $YFe_3Co_8Ti$  compound has a very small uniaxial anisotropy. The  $8j$  sublattice is the major contributor to the uniaxial anisotropy in  $YFe_{11}Ti$ . With all four  $8j$  Fe atoms being replaced by Co atoms in  $YFe_7Co_4Ti$ ,  $K(8j)$  becomes very negative. Moreover,  $K(8i)$  and  $K(8f)$  are also strongly affected and become negative. Further Co doping on  $8f$  sites changes  $K(8i)$  and  $K(8f)$  back to positive in  $YFe_3Co_8Ti$ . Finally, in  $YCo_{11}Ti$  both  $K(8i)$  and  $K(8f)$  increase and  $K(8j)$  becomes less planar, and we have  $K(8i) > K(8f) > 0 > K(8j)$ .

The nonmonotonic composition dependence is often interpreted by preferential site occupancy [59], however, such an explanation is an oversimplification for a metallic system such as  $Y(Fe_{1-x}Co_x)_{11}Ti$ . The MAE contributions from each  $TM$  sublattice may depend on the detailed band structure around the Fermi energy. The doping of Co on particular sites unavoidably affects the electronic structure of neighboring  $TM$  sublattices due to the hybridization between them, which changes the MAE contribution from neighboring sites. Obviously, as shown in Fig. 4, with a sizable amount of Co doping, the variation of anisotropy is a collective effect instead of a sole contribution from the doping sites.

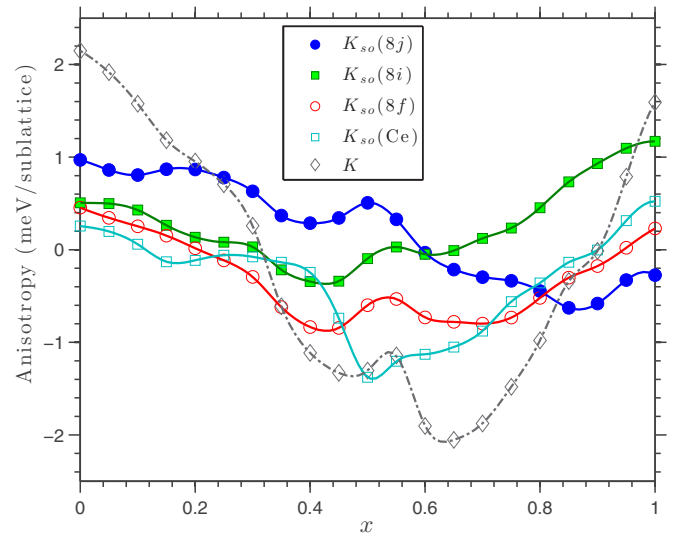
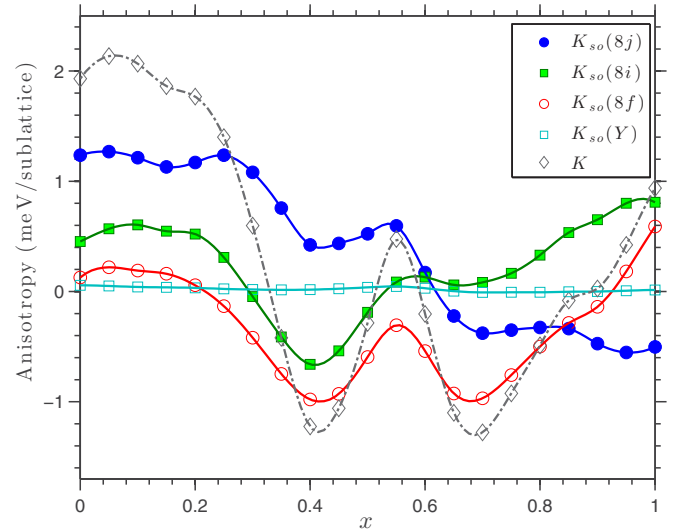


FIG. 5.  $K$  and sublattice-resolved  $K_{so}$  in Y-based (top) and Ce-based (bottom)  $R(Fe_{1-x}Co_x)_{11}Ti$ .

Among three  $TM$  sublattices, the dumbbell  $8i$  sites have the largest contribution to the uniaxial anisotropy in  $YCo_{11}Ti$ , which we found also true in  $CeCo_{11}Ti$ , and hypothetical  $YCo_{12}$  and  $CeCo_{12}$ . It is interesting to compare the MAE contributions from Co sublattices in  $RCO_{12}$  and  $R_2Co_{17}$ , in which the dumbbell Co sites have the most negative contribution to the uniaxial anisotropy [38]. In both cases, the moments of the dumbbell sites prefer to be perpendicular to the dumbbell bonds, which are along different directions in two structures, i.e., basal axes in the 1-12 structure and  $c$  axis in the 2-17 structure. As a result, dumbbell Co sites have MAE contributions of opposite sign in two structures.

In a real sample, Co likely also partially occupies the  $8j$  and  $8f$  sites instead of exclusively only the  $8j$  site. We investigate the scenario at the other extreme by assuming Co occupies the three  $TM$  sublattices with equal probability and calculate composition dependence of MAE using the virtual crystal approximation (VCA). Interestingly, the nonmonotonic behavior is also observed as shown in Fig. 5. The easy

direction changes from uniaxial to in-plane and then back to uniaxial. The variations of each individual  $TM$  sublattice share a similarity with the trend shown in Fig. 4. With increasing of  $x$  in  $\text{Y}(\text{Fe}_{1-x}\text{Co}_x)_{11}\text{Ti}$ ,  $K(8j)$  decreases and becomes negative while  $K(8i)$  and  $K(8f)$  become negative for the intermediate Co composition and then change back to positive at the Co-rich end. Thus, the nonmonotonic behavior is confirmed with or without considering preferential occupancy. The spin-reorientation transition [21] from axis to in-plane occurs in  $\text{Y}(\text{Fe}_{1-x}\text{Co}_x)_{11}\text{Ti}$  but not pure  $\text{YFe}_{11}\text{Ti}$  [21], which may relate to the fact that the competing anisotropies between three  $TM$  sublattices exist in  $\text{Y}(\text{Fe}_{1-x}\text{Co}_x)_{11}\text{Ti}$  while all three  $TM$  sublattices support the uniaxial anisotropy in  $\text{YFe}_{11}\text{Ti}$ . As shown in Fig. 5 (top), MAE in  $\text{Y}(\text{Fe}_{1-x}\text{Co}_x)_{11}\text{Ti}$  barely changes or even slightly increases with a very small Co composition. A similar feature had been observed experimentally [60]. It is caused by the partial occupation of Co on  $8f$  sites in  $\text{YFe}_{11}\text{Ti}$ . We found that replacing Fe atoms in  $\text{YFe}_{11}\text{Ti}$  with Co atoms on the  $8f$  sites increases the MAE.

It is commonly assumed that the MAE contributions from the  $TM$  sublattices are similar in  $R$ - $TM$  compounds with different  $R$ , and such contributions are often estimated experimentally from measurements on corresponding yttrium compounds [12]. As shown in Fig. 5, MAE contributions from  $TM$  sublattices in  $\text{YFe}_{11}\text{Ti}$  and  $\text{CeFe}_{11}\text{Ti}$  are similar but not identical. All three  $TM$  sublattices have positive contributions to the uniaxial anisotropy and  $K(8j) > K(8i) > K(8f) > 0$ . However, magnitudes of each sublattice differ in two compounds, which suggests that the hybridization  $TM$  sites have with different  $R$  atoms affects their contributions to the MAE. Unlike the Y sublattice in  $\text{YFe}_{11}\text{Ti}$ , Ce provides a positive contribution to the uniaxial anisotropy in  $\text{CeFe}_{11}\text{Ti}$ .

#### D. Effect of interstitial doping

Interstitial doping with N, C, and H affects the MAE from both the Fe and  $R$  sublattices [30]. As shown in Table II, H doping barely changes or slightly increases the uniaxial anisotropy in  $\text{YFe}_{11}\text{Ti}$  and  $\text{CeFe}_{11}\text{Ti}$  while carbonizing and nitriding weaken the uniaxial anisotropy, which agrees with experiments [5,27]. Simultaneous substitutional Co doping and interstitial doping with H, C, or N is of interest. Although the uniaxial anisotropy may not improve that much at the low temperature, the effect could be more significant at room temperature. For example, upon hydrogenation, a significant increase of  $K_1$  with a factor 1.8 was observed in  $\text{YFe}_9\text{Co}_2\text{Ti}$  at room temperature [60].

To our knowledge, simultaneous doping of Co and interstitial elements C and N atoms is not well studied. We calculated the MAE dependence on Co compositions in  $\text{Ce}(\text{Fe}_{1-x}\text{Co}_x)_{11}\text{TiZ}$  with  $Z = \text{H}, \text{C}, \text{and N}$ , and results are shown in Fig. 6. The site preference of Co is not considered and VCA is used. The maximum of uniaxial anisotropy in  $\text{Y}(\text{Fe}_{1-x}\text{Co}_x)_{11}\text{TiH}$  is obtained at  $x = 0.1$  while experiments found the maximum at  $\text{YFe}_9\text{Co}_2\text{TiH}$  [60]. For the Fe-rich  $\text{CeCo}_{11}\text{TiZ}$ , only H doping slightly increases the MAE, while C and N quickly decrease uniaxial anisotropy. For  $\text{Y}(\text{Fe}_{1-x}\text{Co}_x)_{11}\text{TiZ}$ , it is unlikely we can have better uniaxial anisotropy (at least at low temperature) over the whole range of Co composition. Interestingly, for Co-rich

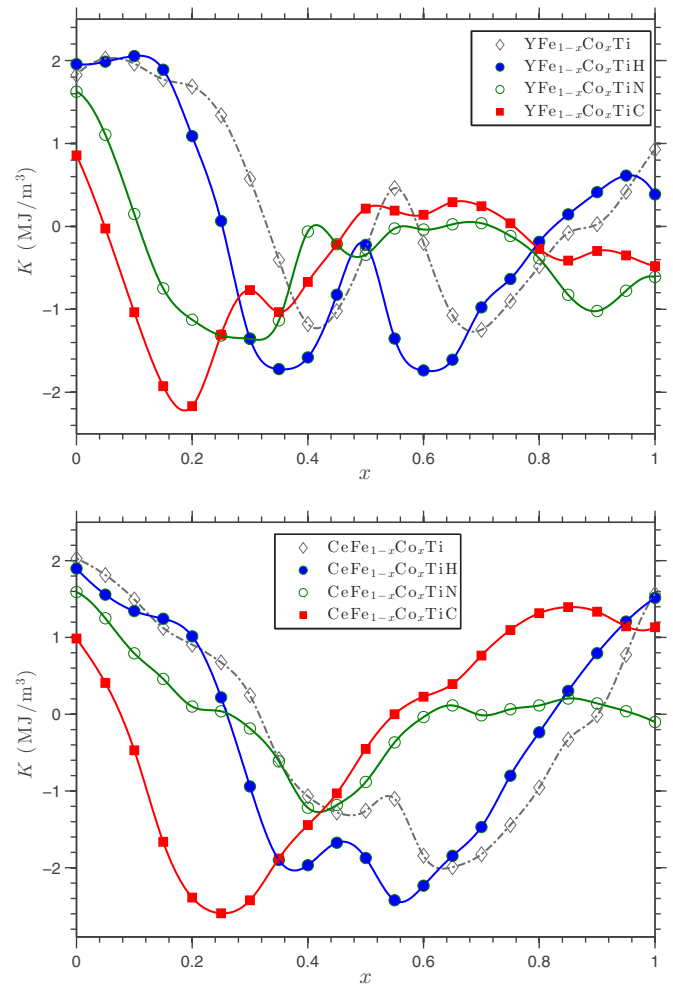


FIG. 6.  $K$  versus Co content in  $R(\text{Fe}_{1-x}\text{Co}_x)_{11}\text{TiZ}$  with  $R = \text{Y}$  (top) and  $R = \text{Ce}$  (bottom), with and without  $Z = \text{H}, \text{C}, \text{and N}$ .

$\text{Ce}(\text{Fe}_{1-x}\text{Co}_x)_{11}\text{TiZ}$ , interstitial C doping significantly improves the uniaxial anisotropy in  $\text{Ce}(\text{Fe}_{1-x}\text{Co}_x)_{11}\text{TiZ}$  for  $0.7 < x < 0.9$ . Considering the relative high Curie temperature on the Co-rich end, it has an attractive combination of all three intrinsic magnetic properties,  $M$ ,  $J$ , and  $K$ , for permanent magnet application.

#### IV. CONCLUSION

Using DFT methods, the intrinsic magnetic properties of  $R\text{Fe}_{11}\text{Ti}$ -related systems were investigated for the effects of substitutional alloying with Co and interstitial doping with H, C, and N. All properties and trends were well described within the local density approximation to DFT. In comparison to the hypothetical  $\text{YFe}_{12}$ , Ti quickly decreases the magnetization and increases the uniaxial magnetic anisotropy in  $\text{YFe}_{11}\text{Ti}$ . The calculated Co site preference is  $8j > 8f > 8i$  in  $\text{Y}(\text{Fe}_{1-x}\text{Co}_x)_{11}\text{Ti}$  with  $x < 0.4$ , in agreement with neutron experiments. The enhancement of  $M$  and  $T_C$  due to Co doping and interstitial doping are in good agreement with experiments.

Compared with  $\text{YFe}_{11}\text{Ti}$ , the calculated  $T_C$  increases by 51, 157, and 211K in  $\text{YFe}_{11}\text{TiZ}$  with  $Z = \text{H}, \text{C}, \text{and N}$ , respectively, with both volume and chemical effects con-



tributing to the enhancement. We found that all three Fe sublattices promote uniaxial anisotropy in the sequence of  $K(8j) > K(8i) > K(8f) > 0$  in  $\text{YFe}_{11}\text{Ti}$ , while competing contributions give  $K(8i) > K(8f) > 0 > K(8j)$  in  $\text{YCo}_{11}\text{Ti}$ . For intermediate Co composition, we confirm that the easy direction changes with increasing Co content from uniaxial to in-plane and then back to uniaxial. Substitutional doping affects the MAE contributions from neighboring sites, and the nonmonotonic composition dependence of anisotropy is a collective effect, which cannot be solely explained by preferential occupancy. The Ce sublattice promotes the uniaxial anisotropy in  $\text{CeFe}_{11}\text{Ti}$  and  $\text{CeCo}_{11}\text{Ti}$ . Interstitial

C doping significantly increases the uniaxial anisotropy in  $\text{Ce}(\text{Fe}_{1-x}\text{Co}_x)_{11}\text{Ti}$  for  $0.7 < x < 0.9$ , which may provide the best combination of all three intrinsic magnetic properties for permanent applications.

#### ACKNOWLEDGMENTS

We thank B. Harmon, A. Alam, C. Zhou, and R. W. McCallum for helpful discussions. This work was supported by the U.S. Department of Energy ARPA-E (REACT 0472-1526). Ames Laboratory is operated for the U.S. DOE by Iowa State University under Contract No. DE-AC02-07CH11358.

- 
- [1] R. McCallum, L. Lewis, R. Skomski, M. Kramer, and I. Anderson, *Annu. Rev. Mater. Res.* **44**, 451 (2014).
- [2] A. Kusne, T. Gao, A. Mehta, L. Ke, M. Nguyen, K. Ho, V. Antropov, C. Wang, M. Kramer, C. Long *et al.*, *Sci. Rep.* **4**, 6367 (2014).
- [3] Y. Yang, L. Kong, S. Sun, D. Gu, and B. Cheng, *J. Appl. Phys.* **63**, 3702 (1988).
- [4] K. Buschow, *J. Magn. Magn. Mater.* **100**, 79 (1991).
- [5] Q. Pan, Z. Liu, and Y. Yang, *J. Appl. Phys.* **76**, 6728 (1994).
- [6] A. Sakuma, *J. Phys. Soc. Jpn.* **61**, 4119 (1992).
- [7] W. Körner, G. Krugel, and C. Elsässer, *Sci. Rep.* **6**, 24686 (2016).
- [8] Y. Yang, H. Sun, Z. Zhang, T. Luo, and J. Gao, *Solid State Commun.* **68**, 175 (1988).
- [9] J. Franse and R. Radwański, *Handbook of Magnetic Materials* (Elsevier, Amsterdam, 1993), Vol. 7, Chap. 5, pp. 307–501.
- [10] H. Li and J. Coey, *Handbook of Magnetic Materials* (Elsevier, Amsterdam, 1991), Vol. 6, Chap. 1, pp. 1–83.
- [11] B. Hu, H. Li, and J. Coey, *J. Appl. Phys.* **67**, 4838 (1990).
- [12] J. Coey, *J. Magn. Magn. Mater.* **80**, 9 (1989).
- [13] F. De Boer, Y. Huang, D. De Mooij, and K. Buschow, *J. Less-Common Met.* **135**, 199 (1987).
- [14] M. Solzi, L. Pareti, O. Moze, and W. David, *J. Appl. Phys.* **64**, 5084 (1988).
- [15] O. Isnard, S. Miraglia, M. Guillot, and D. Fruchart, *J. Alloys Compd.* **275-277**, 637 (1998).
- [16] I. Tereshina, P. Gaczyński, V. Rusakov, H. Drulis, S. Nikitin, W. Suski, N. Tristan, and T. Palewski, *J. Phys. Condens. Matter* **13**, 8161 (2001).
- [17] C. Zhou, F. Pinkerton, and J. Herbst, *J. Appl. Phys.* **115**, 17C716 (2014).
- [18] K. Ohashi, H. Ido, K. Konno, and Y. Yoneda, *J. Appl. Phys.* **70**, 5986 (1991).
- [19] J. Wang, N. Tang, B. Fuquan, W. Wang, W. Wang, G. Wu, and F. Yang, *J. Phys. Condens. Matter* **13**, 1617 (2001).
- [20] V. Sinha, S. Cheng, W. Wallace, and S. Sankar, *J. Magn. Magn. Mater.* **81**, 227 (1989).
- [21] S. Cheng, V. Sinha, B. Ma, S. Sankar, and W. Wallace, *J. Appl. Phys.* **69**, 5605 (1991).
- [22] O. Moze, L. Pareti, and K. Buschow, *J. Phys. Condens. Matter* **7**, 9255 (1995).
- [23] J. Wang, B. Fuquan, C. Yang, and F. Yang, *J. Magn. Soc. Jpn.* **23**, 459 (1999).
- [24] Y. Yang, X. Zhang, L. Kong, Q. Pan, and S. Ge, *Appl. Phys. Lett.* **58**, 2042 (1991).
- [25] Y. Yang, X. Zhang, L. Kong, Q. Pan, S. Ge, J. Yang, Y. Ding, B. Zhang, C. Ye, and L. Jin, *Solid State Commun.* **78**, 313 (1991).
- [26] D. Hurley and J. Coey, *J. Phys. Condens. Matter* **4**, 5573 (1992).
- [27] Q. Qi, Y. Li, and J. Coey, *J. Phys. Condens. Matter* **4**, 8209 (1992).
- [28] Z. Li, X. Zhou, and A. Morrish, *J. Phys. Condens. Matter* **5**, 3027 (1993).
- [29] S. Nikitin, I. Tereshina, V. Verbetsky, and A. Salamova, *Intl. J. Hydrogen Energy* **24**, 217 (1999).
- [30] S. Nikitin, I. Tereshina, V. Verbetsky, and A. Salamova, *J. Alloys Compd.* **316**, 46 (2001).
- [31] D. Zhang, Z. Zhang, Y. Chuang, B. Zhang, J. Yang, and H. Du, *J. Phys. Condens. Matter* **7**, 2587 (1995).
- [32] J. Coey, J. Allan, A. Minakov, and Y. Bugaslavsky, *J. Appl. Phys.* **73**, 5430 (1993).
- [33] J. Chaboy, A. Marcelli, L. Bozukov, F. Baudelet, E. Dartyge, A. Fontaine, and S. Pizzini, *Phys. Rev. B* **51**, 9005 (1995).
- [34] L. Nordström, O. Eriksson, M. Brooks, and B. Johansson, *Phys. Rev. B* **41**, 9111 (1990).
- [35] O. Eriksson, L. Nordström, M. Brooks, and B. Johansson, *Phys. Rev. Lett.* **60**, 2523 (1988).
- [36] A. Alam, M. Khan, R. W. McCallum, and D. D. Johnson, *Appl. Phys. Lett.* **102**, 042402 (2013).
- [37] Y. Wang, J. Shen, N. Chen, and J. Wang, *J. Alloys Compd.* **319**, 62 (2001).
- [38] L. Ke, D. Kukusta, R. W. McCallum, and V. Antropov, in *IEEE Magnetics Conference (INTERMAG)* (IEEE, New York, 2015).
- [39] Z. Li, X. Zhou, and A. Morrish, *J. Appl. Phys.* **69**, 5602 (1991).
- [40] J. Liang, Q. Huang, A. Santoro, J. Wang, and F. Yang, *J. Appl. Phys.* **86**, 2155 (1999).
- [41] O. Andersen, *Phys. Rev. B* **12**, 3060 (1975).
- [42] M. Methfessel, M. van Schilfhaarde, and R. A. Casali, in *Lecture Notes in Physics*, edited by H. Dreyse (Springer-Verlag, Berlin, 2000), Vol. 535.
- [43] A. Mackintosh and O. Andersen, *Electrons at the Fermi Surface* (Cambridge University Press, Cambridge, England, 1980).
- [44] V. Antropov, L. Ke, and D. Åberg, *Solid State Commun.* **194**, 35 (2014).
- [45] L. Ke and M. van Schilfhaarde, *Phys. Rev. B* **92**, 014423 (2015).
- [46] L. Ke, K. Belashchenko, M. van Schilfhaarde, T. Kotani, and V. Antropov, *Phys. Rev. B* **88**, 024404 (2013).
- [47] L. Ke, M. van Schilfhaarde, and V. Antropov, *Phys. Rev. B* **86**, 020402 (2012).
- [48] U. von Barth and L. Hedin, *J. Phys. C* **5**, 1629 (1972).



- [49] P. Haas, F. Tran, and P. Blaha, *Phys. Rev. B* **79**, 085104 (2009).
- [50] G. Kresse and J. Hafner, *Phys. Rev. B* **47**, 558 (1993).
- [51] G. Kresse and J. Furthmüller, *Phys. Rev. B* **54**, 11169 (1996).
- [52] G. Kresse and D. Joubert, *Phys. Rev. B* **59**, 1758 (1999).
- [53] S. Obbade, D. Fruchart, M. Bououdina, S. Miraglia, J. L. Soubeyroux, and O. Isnard, *J. Alloys Compd.* **253**, 298 (1997).
- [54] O. Moze, L. Pareti, M. Solzi, and W. David, *Solid State Commun.* **66**, 465 (1988).
- [55] D. Goll, R. Loeffler, R. Stein, U. Pflanz, S. Goeb, R. Karimi, and G. Schneide, *Phys. Status Solidi (RRL)* **8**, 862 (2014).
- [56] X. Zhao, M. Nguyen, W. Zhang, C. Wang, M. Kramer, D. Sellmyer, X. Li, F. Zhang, L. Ke, V. Antropov *et al.* *Phys. Rev. Lett.* **112**, 045502 (2014).
- [57] J. Trygg, B. Johansson, and M. Brooks, *J. Magn. Magn. Mater.* **104**, 1447 (1992).
- [58] B. Hu, H. Li, J. Gavigan, and J. Coey, *J. Phys. Condens. Matter* **1**, 755 (1989).
- [59] N. Thuy, J. Franse, N. Hong, and T. Hien, *J. Phys. Colloques* **49**, 499 (1988).
- [60] E. Tereshina, I. Telegina, T. Palewski, K. Skokov, I. Tereshina, L. Folcik, and H. Drulis, *J. Alloys Compd.* **404**, 208 (2005).